COORDINATED MICROANALYSIS OF PHOSPHATES IN APOLLO 11 HIGH-TITANIUM BASALTS. J. J. Barnes[1], M. S. Thompson[1], F. M. McCubbin[1], J. Y. Howe[2], Z. Rahman[3], S. Messenger[1], and T. Zega[4]. [1]ARES, NASA JSC, Houston, TX (jessica.j.barnes@nasa.gov). [2]Hitachi High-Technologies America Inc. [3]JETS JACOBS, NASA JSC, Houston, TX. [4] LPL, University of Arizona, Tucson, AZ.

Introduction: Apatite [$Ca_5(PO_4)_3(F,Cl,OH)$] is the main volatile-bearing mineral in lunar rocks. Together with RE-merrillite [$(Mg,Fe)_2REE_2Ca_{16}(PO_4)_{14}$] they make up the primary budget of P on the Moon. The presence of volatiles in lunar apatite has recently been exploited to determine the abundance, distribution, and origin of magmatic lunar volatiles. Notably, some lunar samples have demonstrated a positive correlation between $\delta^{37}Cl$ values and bulk incompatible trace elements (ITEs) and ratios [1-2]. Such trends were interpreted to originate from Cl isotopic fractionation during the degassing of metal chlorides from the lunar reservoir urKREEP (primitive lunar K, P, rare earth element enriched reservoir) during or shortly after the differentiation of the Moon via a magma ocean [1-2].

The goal of our ongoing work is to investigate the inventory and roles of volatiles in the genesis of high-Ti mare basalts. So far, our Cl isotope data [3] indicate that the high-Ti basalts may not have acquired their volatiles from urKREEP. Since the petrological context of apatite (e.g., whether early or late formed) has proven important for interpreting H-isotope data, we are also thoroughly documenting the mineralogical, textural, and structural characteristics of phosphates in Apollo 11 high-Ti basalts.

Samples: We selected samples from high-K and low-K basalt suites that spanned the full range of ITE compositions. Three high-K basalts ('Type A basalts') were studied of bulk K_2O contents between ~0.28 and 0.33 wt.% and La abundances ranging from ~21 to 39 ppm [5-6]. We also studied four low-K basalts, having between 0.05 and 0.11 wt.% K_2O and ~10 and 22 ppm La [5-6].

Methods: Phosphates within the thin sections were located and characterized with the JSC JEOL 7600F scanning electron microscope (SEM). Each thin section was mapped by energy dispersive X-ray spectroscopy (EDS) to locate P hotspots associated with the phosphates. Subsequently, detailed secondary electron and backscattered electron images of individual grains and spot EDS analyses were acquired. Two phosphates were selected for further study by transmission electron microscopy (TEM) and subsequent isotopic imaging using the JSC NanoSIMS 50L. The target crystals were extracted following focused ion beam (FIB) milling using the FEI Quanta 3D dual FEG-SEM at JSC. The FIB sections were then analyzed using the Hitachi HF5000 TEM at LPL, University of Arizona. With the aberration-corrected HF5000, equipped with and large-area twin EDS detectors with 1.8 SR solid angle, we were able to collect high-resolution EDS X-ray maps of the FIB sections in less than 30 minutes. We also performed selected-area electron-diffraction (SAED) analyses for mineral identification and determination of crystal structure.

Textural analysis of Apollo 11 phosphates: Phosphates occur as a late-stage crystallization product, almost exclusively in mesostasis areas within the samples we investigated. Apatite is present either as (i) discrete crystals varying from basal to acicular, while most are euhedral with some being subhedral, and (ii) apatite-merrillite intergrowths. Backscattered electron images of some apatite in high-Ti mare basalts indicate strong chemical zoning (Fig. 1a). The intergrowths vary in texture from hexagonal crystals containing both phosphates (typically within the mesostasis) to vein-like merrillite with minor anhedral apatite. The latter are more commonly located at the boundary of, or cross-cutting through the main rock-forming minerals (e.g. pyroxene). The observed intergrowth textures are strikingly similar to those reported in lunar highlands samples and KREEP-rich basalts [e.g., 4,7]. We also noted that apatite in Type-A basalts commonly contains a symplectitic intergrowth with another mineral of high backscatter contrast (Fig. 1b), but the features were too fine-scale (< 1µm) to be chemically identified by SEM.

One concentrically-zoned apatite crystal from low-K basalt 10029 (hereafter Phosphate#1) and one apatite-merrillite intergrowth with symplectite features from high-K basalt 10024 (hereafter Phosphate#2) were chosen for further study by TEM and NanoSIMS.

Fractional crystallization of lunar apatite: The high-resolution EDS data from the TEM reveals that Si, REEs, and Cl all increase from core-to-rim of Phosphate#1 whilst there is a corresponding decrease in both Ca and P from core-to-rim (Fig. 2). The Y+Nd+Ce content of apatite varies from ~3 to ~30 wt.% from core-to-rim. The SAED results indicate that the apatite is orientated such that we are looking down the C-axis. Most importantly, the crystal orientation does not change from core-to-rim, even in the outermost zone (brightest zone Fig. 1a). The structural analyses indicate that the apatite captured in the FIB section is one crystal that likely grew continuously rather

than the zones representing later overgrowths. Overall, the results obtained suggest that this crystal was formed by fractional crystallization, most likely by a coupled substitution: $P^{5+} + Ca^{2+} \leftrightarrow Si^{4+} + REE^{3+}$ [e.g., 8]. As predicted by the apatite fractional crystallization model [e.g., 9], the Cl abundance of the apatite is highest in the rim of the grain while F is lowest in the rim. This crystal will be analyzed by NanoSIMS to more accurately determine the distribution of volatiles and REEs from core to rim.

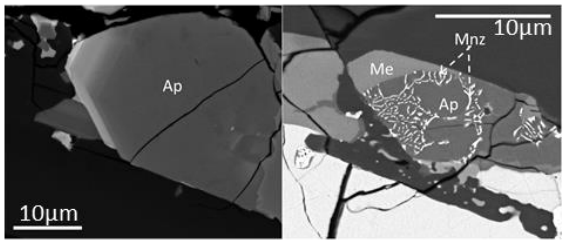

Figure 1. Backscattered electron images of the phosphates that were studied by coordinated microanalysis. *Left:* zoned apatite (Ap) from 10029. *Right:* Symplectic assemblage of Ap, merrillite (Me), and monazite (Mnz) in 10024.

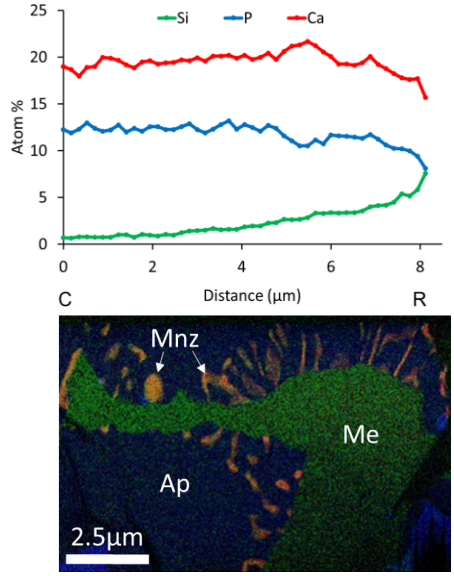

Figure 2. TEM data (top) Core-to-rim EDS chemical composition profiles of Phosphate#1 and (bottom) false color X-ray map of Phosphate#2 (G=Mg, B=F, R=Ce).

Monazite in lunar basalts: TEM EDS data for Phosphate#2 indicate that the mineral forming a symplectite assemblage with apatite (Fig. 1b) is likely monazite [(Y,REE)PO_4] or a monazite-like phase (Fig. 2). SAED patterns also indicate that this could be monazite. We are in the process of acquiring nano-diffraction data to more robustly confirm this observation.

Lunar monazite has been reported previously [10-12], however, to our knowledge, texturally-similar monazite inclusions to those we identified have yet to be reported in lunar samples. Monazite inclusions in apatite in Martian meteorite NWA 7034 were reported by Liu et al. [13], and they interpreted those occurring in the matrix to be of hydrothermal or metasomatic origin. Of the samples we have investigated, symplectitic monazite has only been found in the ITE-enriched high-K mare basalts. These features may thus represent exsolution of monazite from apatite based on the high temperatures and high REE abundances in the melt at the time of basalt crystallization. We are further investigating the physicochemical implications of apatite-monazite symplectite formation.

Conclusions: Our results are consistent with chemical zonation of apatite being the result of coupled substitution between apatite and residual melts. Unidirectional crystal orientation indicates that the particular crystal studied was formed by continual growth rather than secondary mineral formation. Thus, we posit that Phosphate#1 and other texturally similar apatites are the product of fractional crystallization in absence of RE-merrillite [14]. Fractional crystallization of apatite has also been used to explain the F,Cl,OH systematics of late-stage apatite in lunar basalts [9]. We have observed symplectitic monazite in the ITE-enriched high-K basalts, and the texture indicates that monazite exsolved from apatite in those basalts, possibly during cooling.

Acknowledgments: This work is supported by a NASA postdoctoral fellowship awarded to JJB and NASA's LASER program grant #NNX13AK32G awarded to FMM. We thank CAPTEM for allocating Apollo samples to this project. We gratefully acknowledge NASA (grants #NNX12AL47G and #NNX15AJ22G) and NSF (grants #1531243 and #0619599) for funding of instrumentation in the Kuiper Materials Imaging and Characterization Facility.

References: [1] Boyce J. W. et al. (2015) *Sci. Adv., 1*, e1500380. [2] Barnes J. J. et al. (2016) *EPSL* 447, 84-94. [3] Barnes J. J. et al. (2017) *Proc. LPSC XLVIII #1727.* [4] Tartèse R. et al. (2014) *Geology* 42, 363-366. [5] Meyer, C. (2012). Lunar Sample Compendium, and references therein. [6] Hallis L. J. et al. (2014) *GCA* 134, 289-316. [7] Elardo S. et al. (2012) *GCA* 87, 154-177. [8] Rønsbo J. G. (1989) *Amer. Min.* 74, 896-901. [9] Boyce J. W. et al. (2014) *Science* 344, 400-402. [10] Lovering J. F. et al. (1972) Proc. LSC, 493-494. [11] Jolliff B. L. (1994) *Proc. LPSC XXIV, 724.* [12] Kartashov P.M. et al. (2005) *DES 407A.* [13] Liu Y. et al. (2016) *EPSL* 451, 251-262. [14] Jolliff B. L. et al. (1993) *GCA* 57, 4069-4094.